Supplementary Information

Highly Anisotropic and Water Molecule-Dependent Proton Conductivity in a 2D Homochiral Copper(II) Metal–Organic Framework

Rong Li,[a,b] Shuai-Hua Wang,[a] Xu-Xing Chen,[a] Jian Lu,[a,b] Zhi-Hua Fu,[a] Yan Li,[c] Gang Xu,[a] Fa-Kun Zheng,[a,*] and Guo-Cong Guo[a,*]

[a] *State Key Laboratory of Structural Chemistry, Fujian Institute of Research on the Structure of Matter, Chinese Academy of Sciences, Fuzhou, Fujian 350002, P. R. China*

[b] *University of Chinese Academy of Sciences, Beijing 100039, P. R. China*

[c] *Department of Chemistry, East China University of Science and Technology, Shanghai 200237, P. R. China*

Table S1. Selected lengths (Å) and angles (º) for the as-synthesized crystals of **1·3H$_2$O** at room temperature

1·3H$_2$O			
Cu(1)–O(12)#1	1.960(3)	Cu(1)–N(21)	2.038(3)
Cu(1)–N(14)#1	1.981(3)	Cu(1)–N(15)#1	2.067(3)
Cu(1)–N(12)	2.297(4)	N(15)–Cu(1)#2	2.067(3)
N(14)–Cu(1)#2	1.981(3)	O(12)–Cu(1)#2	1.960(3)
O(12)#1–Cu(1)–N(14)#1	172.37(14)	O(12)#1–Cu(1)–N(15)#1	82.48(12)
O(12)#1–Cu(1)–N(21)	90.45(13)	N(14)#1–Cu(1)–N(15)#1	93.13(13)
N(14)#1–Cu(1)–N(21)	91.79(14)	N(21)–Cu(1)–N(15)#1	160.94(13)
N(14)#1–Cu(1)–N(12)	93.04(14)	O(12)#1–Cu(1)–N(12)	93.94(13)
N(21)–Cu(1)–N(12)	96.80(14)	N(15)#1–Cu(1)–N(12)	101.31(14)

Symmetry codes for **1·3H$_2$O**: #1 $-x + 1/2$, $y + 1/2$, $-z + 1$; #2 $-x + 1/2$, $y - 1/2$, $-z + 1$; #3 $-x$,

$-y + 1, z$.

Table S2. Selected lengths (Å) and angles (°) for **1** at 80 °C under N_2 atmosphere

1			
Cu(1)–O(12)#1	1.947(3)	Cu(1)–N(21)	2.031(4)
Cu(1)–N(14)#1	1.972(3)	Cu(1)–N(15)#1	2.049(4)
Cu(1)–N(12)	2.394(4)	N(15)–Cu(1)#2	2.049(4)
N(14)–Cu(1)#2	1.972(4)	O(12)–Cu(1)#2	1.947(3)
O(12)#1–Cu(1)–N(14)#1	174.19(17)	O(12)#1–Cu(1)–N(15)#1	82.15(15)
O(12)#1–Cu(1)–N(21)	91.47(15)	N(14)#1–Cu(1)–N(15)#1	92.82(15)
N(14)#1–Cu(1)–N(21)	92.77(16)	N(21)–Cu(1)–N(15)#1	165.71(16)
N(14)#1–Cu(1)–N(12)	90.97(15)	O(12)#1–Cu(1)–N(12)	92.81(15)
N(21)–Cu(1)–N(12)	92.44(16)	N(15)#1–Cu(1)–N(12)	100.60(15)

Symmetry codes for **1**: #1 $-x + 1/2, y + 1/2, -z + 1$; #2 $-x + 1/2, y - 1/2, -z + 1$; #3 $-x, -y + 1, z$.

Table S3. The main hydrogen bonds for **1·3H$_2$O**

D–H···A	D–H (Å)	H···A (Å)	D···A (Å)	<(DHA) (°)
O1W–H1WA...O12_$1	0.848(14)	2.35(7)	3.114(8)	155(12)
O1W–H1WA...O11_$1	0.849(14)	2.46(7)	3.255(8)	156(12)
O1W–H1WB...O1_$2	0.847(14)	2.28(8)	2.992(11)	141(12)
O2W–H2WA...O1_$3	0.853(14)	2.08(2)	2.71(2)	130.6(7)
O2W–H2WA...O1	0.853(14)	2.08(2)	2.71(2)	130.6(7)
O1–H1A...O2W	0.82	1.89	2.71(2)	174.9

Symmetry codes: $1 0.5 $-x, y + 1.5, 1 - z$; $2 $-x, -y, z - 1$; $3 $-x, -y - 2, z$.

Table S4. Properties of selected transitions and their contributions of **1·3H$_2$O**

State	Transition Energy (eV)	Oscillator *f*	Rotational strength *R*	Contributions
4	1.73	0.0119	–3.6468	227–230 (84%)
8	1.85	0.0124	–9.8035	224–230 (35%)
				228–230 (16%)
22	2.70	0.0286	+28.8284	204–230 (13%)
				207–230 (13%)
22	2.70	0.0286	+28.8284	201–230 (11%)
24	2.77	0.0280	+46.4047	212–230 (26%)
				215–230 (25%)

Table S5. The proton conductivity (σ) and activation energy (*E*a) of the representative microcrystalline samples of 2D MOFs

References		Conditions	σ/S cm^{-1}	E_a/eV
J. Am. Chem. Soc., 2009, 131, 9906(S1)	pellets	307 K, 98%RH	8×10^{-3}	0.63
Chem. Commun., 2013, 49, 6197(S2)	pellets	300 K, 98% RH	3.4×10^{-3}	
J. Am. Chem. Soc., 2010, 132, 14055(S3)	pellets	298 K, 95% RH	3.5×10^{-5}	0.17
Chem. Eur. J., 2015, 21, 13793(S4)	pellets	300 K, 95% RH	1.5×10^{-5}	0.52
Cryst. Growth Des., 2014, 14, 310(S5)	pellets	298 K, 98% RH	1.3×10^{-5}	0.52
Chem. Commun., 2012, 48, 4998(S6)	pellets	298 K, 98% RH	8.58×10^{-6}	0.23
Bull. Chem. Soc. Jpn., 1979, 52, 3296(S7)	pellets	300 K, 100% RH	2.2×10^{-6}	0.16
Inorg. Chem. Commun., 2003, 6, 346(S8)	pellets	300 K, 75% RH	10^{-6}	
Inorg. Chem., 2015, 54, 1218(S9)	pellets	353 K, 95% RH	2.55×10^{-7}	0.96
J. Am. Chem. Soc., 2013, 135, 2256 (S10)	pellets	298 K, 65% RH	1.0×10^{-7}	
J. Am. Chem. Soc. 2014, 136, 12444(S11)	single crystal	353 K	9.02×10^{-5}	0.47
J. Am. Chem. Soc. 2012, 134, 12780(S12)	single crystal	403 k	1.1×10^{-4}	0.6

J. Am. Chem. Soc. 2014, 136, 9292(S13)	single crystal	298K, 95% RH	3.05×10^{-4}	0.34
Chem. Commun., 2014, 50, 1144	pellets	298 K, 60% RH	3.9×10^{-4}	
CrystEngComm, 2014, 16, 64	pellets	298 K, 95% RH	5.42×10^{-7}	0.39
Eur. J. Inorg. Chem., 2016, 4476	pellets	298 K, 95% RH	1.40×10^{-4}	0.54,
Inorg. Chem., 2013, 52, 12131	pellets	413 K, 95% RH	1×10^{-3}	0.1
Inorg. Chem., 2016, 55, 8971	pellets	293 K, 99% RH	1.64×10^{-3}	0.22
Inorg. Chem., 2016, 55, 7414	pellets	353 K, 95% RH	3×10^{-4}	0.20 – 0.33
J. Am. Chem. Soc., 2009, 131, 13516	pellets	298 K, 75% RH	1×10^{-4}	
J. Am. Chem. Soc., 2012, 134, 5472	pellets	298 K, 75% RH	1×10^{-4}	
J. Am. Chem. Soc., 2012, 134, 19432	pellets	298 K, 95% RH	2.3×10^{-3}	0.22
Chem. Sci., 2013, 4, 983	pellets	298 K	4.1×10^{-4}	0.21

Table S6. The parameters for the best fit of the data, activation energies (*E*a) and proton conduction mechanism of **1·3H$_2$O** along [100] and [010] directions.

direction	R^2	slope	E_a /eV	proton conduction mechanism
[100]	0.98	–5.59	0.48	Vehicle mechanism
[010]	0.99	–6.54	0.56	Vehicle mechanism

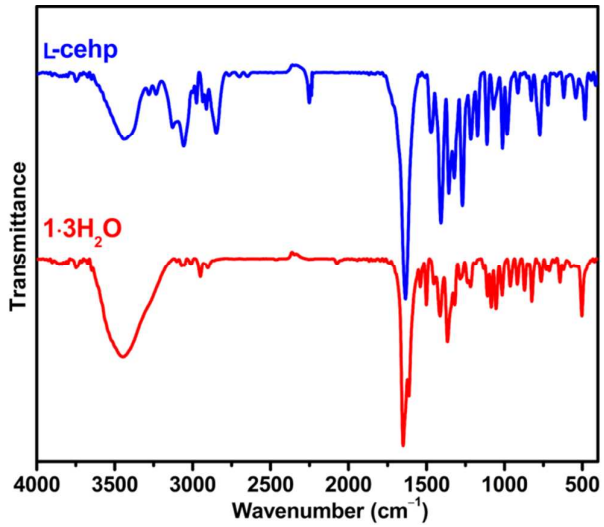

Figure S1. The FT-IR spectra of L-cehp and compound **1·3H$_2$O**.

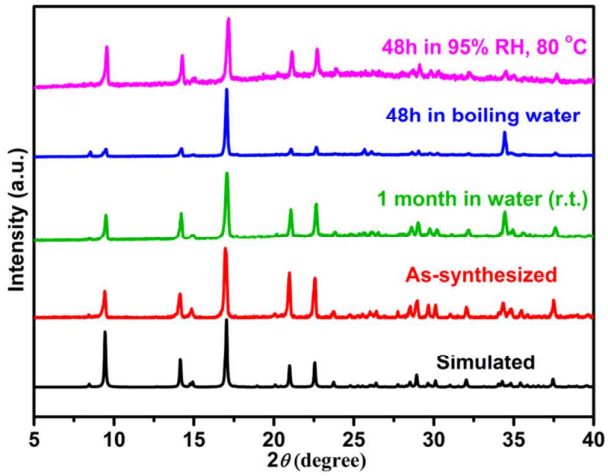

Figure S2. Comparison of experimental PXRD patterns for **1·3H$_2$O** obtained under different conditions with its simulated one derived from single-crystal X-ray data.

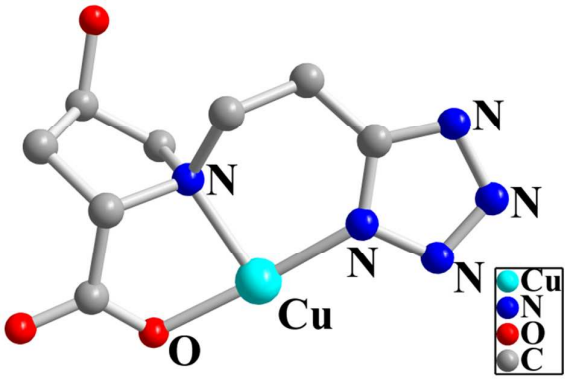

Figure S3. A tridentate fac mode with *N*-[2-(1*H*-tetrazol-5-yl)ethyl]-L-hydroxyproline binding to Cu(II).

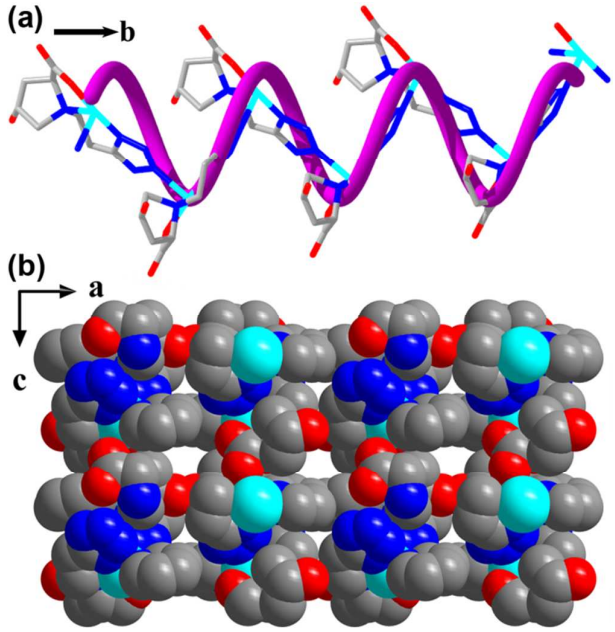

Figure S4. (a) The 1D helix chain of **1·3H$_2$O** and the idealized pink helix; (b) The stacking structure of **1·3H$_2$O** with 9.5% solvent-accessible volume.

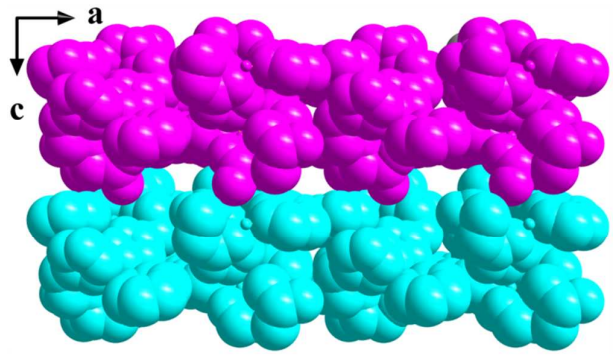

Figure S5. The stacking direction of the supramolecular 3D framework along the *c*-axis with the pink and cyan balls representing the 2D networks parallel to the *ab* plane.

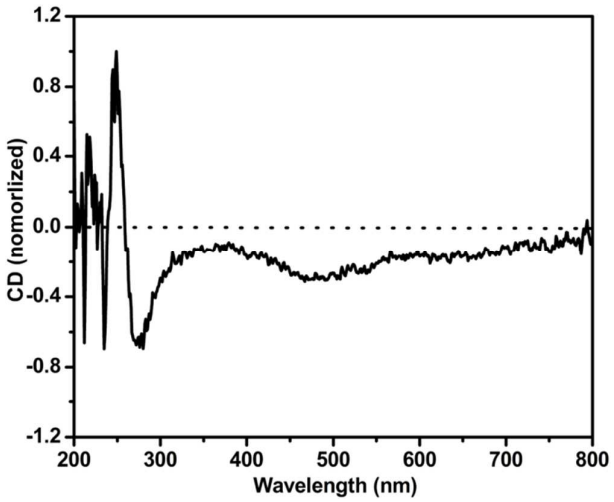

Figure S6. The solid-state experimental CD spectra of L-cehp.

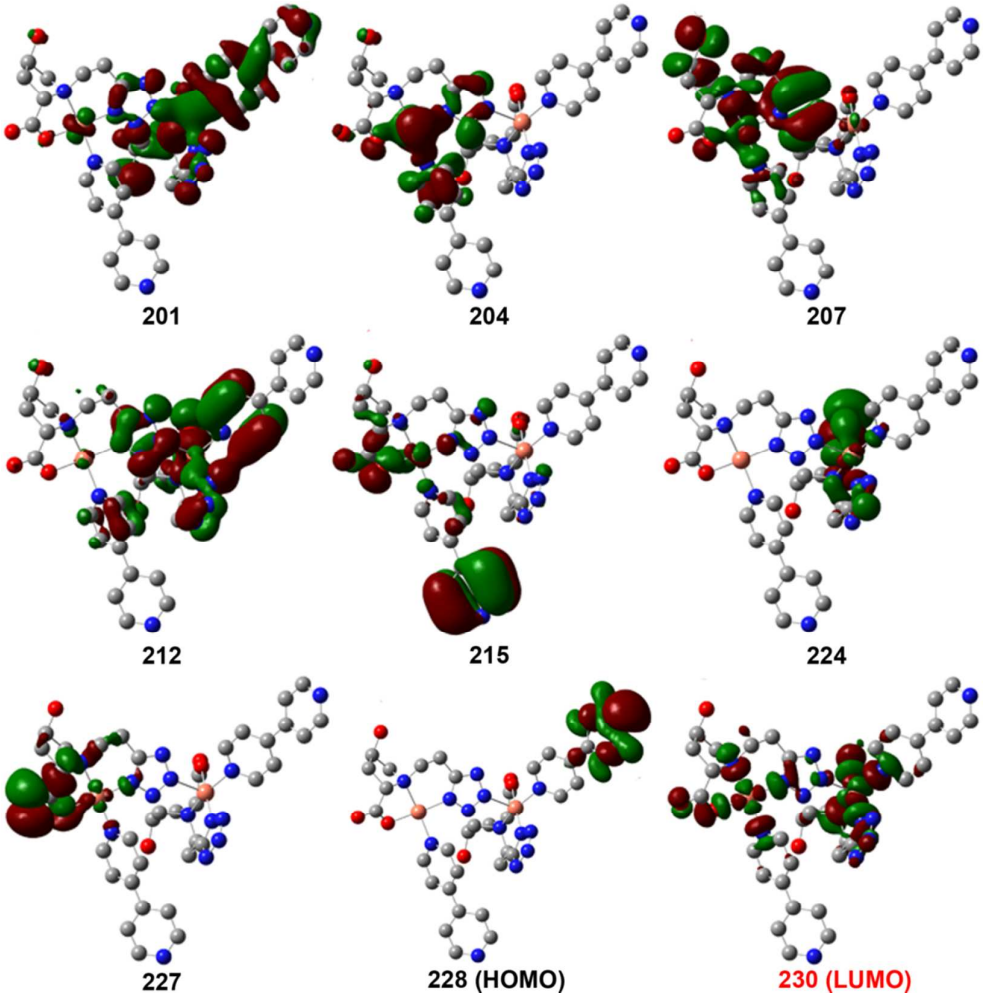

Figure S7. Molecular orbitals associated with the main transitions in **1·3H_2O**. Labels for the occupied and virtual orbitals are indicated in black and red, respectively.

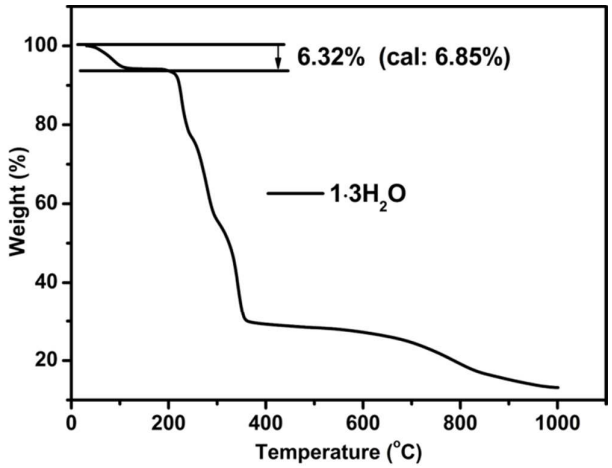

Figure S8. TGA curve for **1·3H$_2$O**.

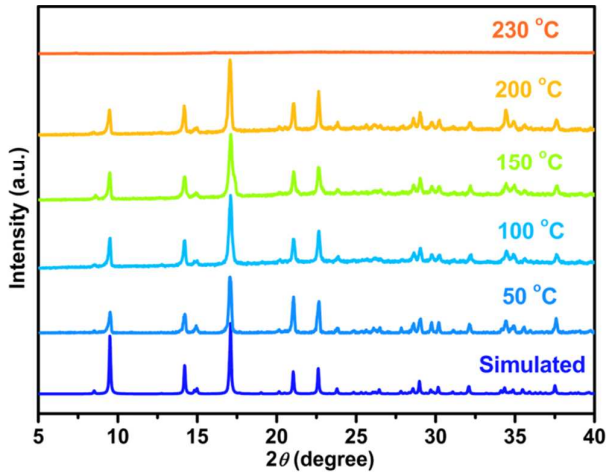

Figure S9. Comparison of experimental PXRD patterns for **1·3H$_2$O**, being heated for 1 h in the oven at each temperature point in the air atmosphere (RH > 70 %), with its simulated one from single-crystal X-ray data.

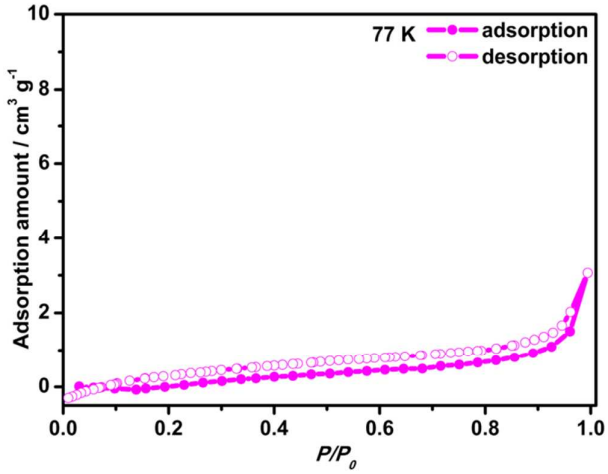

Figure S10. Nitrogen gas adsorption/desorption isotherms of **1** (77 K).

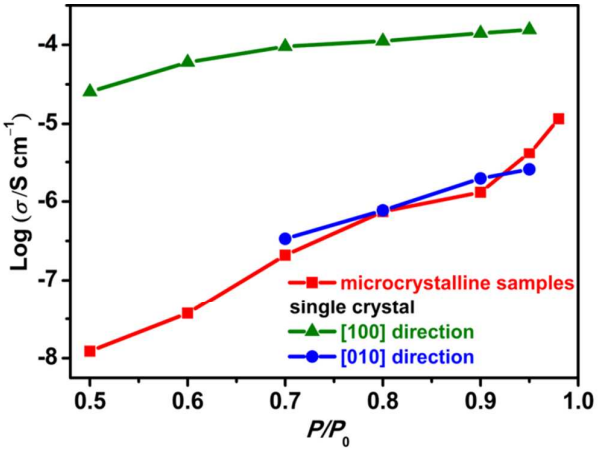

Figure S11. Humidity-dependence proton conductivity of microcrystalline samples, and single crystals along [100] and [010] directions measured at 30 ^{o}C.

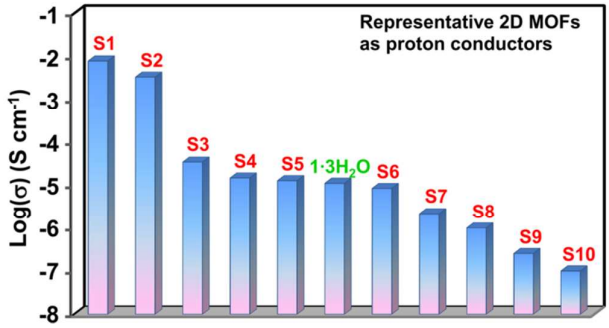

Figure S12. The comparison of proton conductivity of microcrystalline sample **1·3H$_2$O** with representative microcrystalline 2D MOFs at low temperature and high humidity. The proton conductivities of compounds **S1–S10** are listed in Table S5.

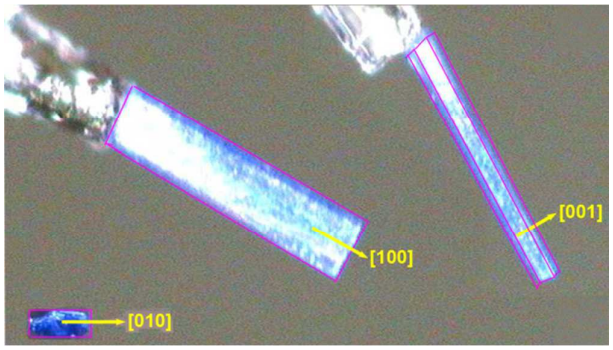

Figure S13. The determined single crystal directions of [100], [010] and [001] of **1·3H$_2$O** on the SuperNova CCD diffractometer.